HHS Public Access

Author manuscript

J Memb Sci. Author manuscript; available in PMC 2019 June 01.

Published in final edited form as:

J Memb Sci. 2018 June ; 555: 348–361. doi:10.1016/j.memsci.2018.03.060.

Role of membrane pore polymerization conditions for pH responsive behavior, catalytic metal nanoparticle synthesis, and PCB degradation

Md. Saiful Islam[a], **Sebastián Hernández**[a], **Hongyi Wan**[a], **Lindell Ormsbee**[b], and **Dibakar Bhattacharyya**[a,*]

[a]Department of Chemical and Materials Engineering, University of Kentucky, 177 F. Paul Anderson Tower Building, Lexington, KY 40506, USA

[b]Department of Civil Engineering, University of Kentucky, Lexington, KY 40506, USA

Abstract

This article describes the effects of changing monomer and cross-linker concentrations on the mass gain, water permeability, Pd-Fe nanoparticle (NP) loading, and the rate of degradation of 3,3',4,4',5-pentachlorobiphenyl (PCB 126) of pore functionalized polyvinylidene fluoride (PVDF) membranes. In this study, monomer (acrylic acid (AA)) and cross-linker (N, N′- methylene-bis (acrylamide)) concentrations were varied from 10 to 20 wt% of polymer solution and 0.5–2 mol% of monomer concentration, respectively. Results showed that responsive behavior of membrane could be tuned in terms of water permeability over a range of 270–1 L m^{-2} h^{-1} bar^{-1}, which is a function of water pH. The NP size on the membrane surface was found in the range of 16–23 nm. With increasing cross-linker density the percentage of smaller NPs (< 10 nm) increases due to smaller mesh size formation during in-situ polymerization of membrane. NP loading was found to vary from 0.21 to 0.94 mg per cm^2 of membrane area depending on the variation of available carboxyl groups in membrane pore domain. The NPs functionalized membranes were then tested for use as a platform for the degradation of PCB 126. The observed batch reaction rate (K_{obs}) for PCB 126 degradation for per mg of catalyst loading was found 0.08–0.1 h^{-1}. Degradation study in convective flow mode shows 98.6% PCB 126 is degraded at a residence time of 46.2 s. The corresponding surface area normalized reaction rate (K_{sa}) is found about two times higher than K_{sa} of batch degradation; suggesting elimination of the effect of diffusion resistance for degradation of PCB 126 in convective flow mode operation. These Pd-Fe-PAA-PVDF membranes and nanoparticles are characterized by TGA, contact angle measurement, surface zeta potential, XRD, SEM, XPS, FIB, TEM and other techniques reveal the details about the membrane surface, pores and nanoparticles size, shape and size-distribution. Statistical analysis based on experimental

*Corresponding author. db@uky.edu (D. Bhattacharyya).

Appendix A. Supplementary material

The supplementary material includes: Zeta potential plot, Water flux profile of different batches of membrane, TEM images of solution phase Fe nanoparticles, EDS spectrum of solution phase Fe nanoparticles, XRD pattern of solution phase Pd-Fe nanoparticles, FIB image of the top surface of Pd-Fe-PAA-PVDF membrane, STEM images and EDS spectrum of the inner sections of Pd-Fe-PAA-PVDF membrane, Elemental mapping inside the Pd-Fe-PAA-PVDF membrane, EDS analysis conducted inside of the Pd-Fe-PAA-PVDF membrane, Solution phase degradation of PCB 126, Factorial design analysis, Interaction and main (individual) effects of monomer and cross-linker concentration on mass gain (%) and permeability ratio (A_{min}/A_{max}), Response surface design analysis. Supplementary data associated with this article can be found in the online version at http://dx.doi.org/10.1016/j.memsci.2018.03.060.

results allows us to depict responsive behavior of functionalized membrane. In our best knowledge this paper first time reports detail study on responsive behavior of pore functionalized membrane in terms of permeability, NPs size, metal loading and its effect on PCB 126 degradation in a quantified approach.

1. Introduction

To address the global challenge of water contamination, membrane-based separation methods are being increasingly studied for potential applications for water purification [1,2]. Current advancements in developing functionalized membranes with porous support and different functional polymers, opens-up the possibility to fine-tune the pore structure, permeability (A) and selectivity of the membranes [3–5]. In particular, cross-linked hydrophilic polymers are being studied in different functionalization processes, especially in the preparation of responsive membranes [6,7]. As diverse membrane separation processes typically require different pH environments, the demand for functionalized pH responsive membranes has increased [8]. Using pH responsive polymers, such as polyacrylic acid (PAA), poly (methylacrylic acid), poly (vinylpyridine) etc., along with a suitable cross-linker, make it possible to functionalize pH responsive membranes [8,9]. Further, incorporation of catalytic nanoparticles (NPs) across the pores of the modified surface of the membrane provides an effective platform for in situ surface reactions in different pH environments [10,11].

Chlorinated organic compounds (COCs) are a serious concern as environmental pollutants due to their high toxicity, chemical stability and presence in soils, sediments as well as in different water sources [11–13]. Nano scale zero valent iron (nZVI) and iron based bimetallic NPs have been intensively studied for the degradation of COCs into less toxic or nontoxic products [14–21]. The addition of a second metal such as Pt, Pd, Au, Ag, Ni, Cu, Zn with Fe will enhance the catalytic activity for dichlorination [22–24]. Among these metals, Pd is well known and the most studied catalyst for hydro-dechlorination of COCs due to its noble nature [25,26]. When bimetallic Pd-Fe is used in COCs degradation in water, Fe acts as an electron source and Pd as a catalyst. Once, hydrogen is produced from nZVI due to its corrosion in water, it is activated by Pd to form highly reactive hydrogen radicals. These hydrogen radicals then serve as effective electron donors for dechlorination of COCs, whether Pd is coated on nZVI or is present as separate NPs [27]. Incorporation of these reactive NPs in membrane results as a suitable platform for water remediation and antifouling application. Different methods for in situ preparation of nanoparticle-based membrane systems for water remediation are well documented in literature [20]. In our previous studies, we reported the synthesis of Fe, Pd-Fe, Ni-Fe, and iron oxide immobilized in polyvinylidene fluoride/poly (acrylic acid) (PVDF-PAA) membranes for use in the degradation of COCs [28–32]. These functionalized membranes have been used as porous supporting materials to control NPs aggregation, to capture dissolved metal ions, and to perform batch and convective flow degradation studies of COCs through the associate membrane pores. During functionalization, monomer (M) and cross-linker (X) concentrations play a significant role in the functionalization of the membrane pore matrix.

They also have influences on NPs loading [7,33,34]. However, the impact of monomer and cross-linker concentrations has not been addressed in previous works.

The main purpose of this study is to investigate the effects of M and X concentrations on the performance of pore functionalized pH responsive membranes for water-based dechlorinations applications, using 3,3',4,4',5-pentachlorobiphenyl (PCB 126) as a model compound. The specific objectives of this work are: i) to functionalize PVDF membranes using different combinations in concentrations of PAA as a monomer, M (wt%), and (N, N′-methylenebis (acrylamide)) (MBA) as a cross-linker, X (mol%), ii) to study the variation of responsive behavior of PAA-PVDF membrane and understand its effects on mass gain, water permeability, Pd-Fe NPs size and metal loading, iii) to depict the details of Pd-Fe-PAA-PVDF membranes and nanoparticles by TGA, contact angle measurement, surface zeta potential, XRD, SEM, XPS, FIB, TEM and other characterization techniques and finally, iv) to investigate the reaction kinetics of Pd-Fe NPs through the reduction of PCB 126. Details of specific objectives are portrayed in Scheme 1.

2. Materials and methods

2.1. Materials

All chemicals used during the laboratory-scale membrane functionalization and the other studies were reagent grade and used without further purification. Acrylic acid (AA, 98%), N, N′-methylenebis (acrylamide) (MBA, 99%) and sodium borohydride (98%) were received from ACROS ORGANICS. Potassium persulfate (KPS,>99%) was procured from EM SCIENCE. Potassium tetrachloropalladate(II) (99%) was purchased from STREM Chemicals. Naphthalene_d_8 (99 atom% D) was purchased from Sigma-Aldrich. Sodium hydroxide (0.1 N), sulfuric acid (0.5 M), hydrochloric acid (0.1 N), hexanes (> 99%) and ferrous chloride tetrahydrate (> 99%) were obtained from Fisher Scientific. 3,3',4,4',5-pentachlorobiphenyl (PCB 126) (> 97%, neat) and biphenyl (> 97%, neat) along with their analytical solution (100 ppm in hexane) were acquired from Ultra Scientific. Ethyl alcohol and methanol were bought from EMD Millipore Corporation. Sodium chloride (99%) was purchased from Alfa Aesar. Full scale PVDF microfiltration membranes (PV700, pore diameter of 250–400 nm, thickness around 172 ± 5 μm and porosity around 38–46%) were obtained from Nanostone Water, Inc.

2.2. Functionalization of PVDF membranes

Lab scale PVDF membranes were functionalized via an in-situ polymerization method, as reported before [31,35]. Before functionalization, membranes were soaked in methanol for 5–10 min to remove dirt, clean the pores and increase the hydrophilicity of the surface [36]. After that a mixture of monomer solution (pH = 5.5–5.6) of AA (10–20 wt% aqueous solution) with MBA as the cross-linker (0.5–2.0 mol% of AA), and KPS as an initiator (1.0 mol% of AA) was passed through the membrane under vacuum (0.14–0.16 bar vacuum) [37]. The solution was passed 3–4 times through the top surface of the membrane and once through the back of the membrane to confirm a homogenous polymerization across the pores. The membranes were then baked at 70–75 °C for 1–1.5 h under N_2 atmosphere or vacuum. This allows functionalization of the membrane via a thermal initialized

polymerization of AA inside the PVDF membrane pores. After that, functionalized membranes were washed thoroughly with deionized ultrafiltered (DIUF) water to eliminate any unreacted constituents and then dried for 30 min at around 50–55 °C. Finally, the membranes were weighed to confirm polymerization through mass gain. In Fig. 1 a step by step process of the functionalization of the PVDF membrane, the Pd-Fe NP loading, and the degradation of PCB 126 solution using a Pd-Fe-PAA-PVDF membrane is depicted.

In order to study the effects of M and X concentrations, six different batches of functionalized membranes were prepared. M concentration was varied from 10 to 20 wt% of solution, and X concentration was varied from 0.5 to 2 mol% of monomer concentration. In our previous studies we have taken monomer concentration to vary from 10 to 20 wt % with 1 mol% of cross-linker concentration [31,38–40]. However, in those studies we have not addressed the effect that M and X have on mass gain, permeability (A), metal loading, NP size and degradation of COCs (in this case, PCB 126) besides membrane characterizations. In this study, we have extended the variation of cross-linker concentration in the range of 0.5–2 mol% of monomer concentration. For all the prepared batches of membrane, the initiator (KPS), concentration was kept constant to 1 mol% of M concentration in polymer solution. In Table 1 the matrix of chemicals used for preparing different batches of pore functionalized membranes to evaluate the effect of monomer and cross-linker concentration variation is shown.

2.3. Nanoparticle immobilization in functionalized membranes

In-situ immobilization of Fe and Pd NPs in the functionalized membrane pores was achieved by first doing ion exchange followed by reduction of Fe and subsequent Pd coating as reported in previous works [38,40]. For cation exchange, PVDF-PAA membranes were soaked in NaCl (~ 68 mM) solution (pH ≥ 10). The ionized carboxyl groups chelated with Na^+ while releasing H^+ to cause a decrease in the pH of the solution. Therefore, to maintain the pH, NaOH was added in intervals. After 12–14 h, (solution pH > 8), the membranes were then washed with deoxygenated water to remove any excess NaCl/NaOH from the pores. For a second ion exchange, the membrane was put into a dead-end filtration cell. Then, 200 mL of $FeCl_2$ solution (~ 3.57 mM, pH = 5.0–5.5) was passed through under N_2 pressure (2–3 bar). This convective mode operation allows all Na^+ ions to be replaced by Fe^{2+}, thereby forming iron-carboxylate conjugates both in the surface and inside the pores. In the reduction step, Fe^{2+} was immediately reduced to zerovalent iron NPs by passing 300 mL of $NaBH_4$ solution (~ 26 mM) under N_2 pressure (3–5 bar) through the membrane. Finally, the immobilization of Pd NPs on Fe surface was achieved by passing 200 mL (ethanol:water = 9:1 v/v) of K_2PdCl_4 solution (~ 153 μM, Pd as 1 wt% of Fe) through the Fe-PAA-PVDF membrane under N_2 pressure (2–4 bar). This step was repeated until the K_2PdCl_4 solution turned colorless. This ensures all Pd^{2+} were reduced by Fe°, forming Pd° and Fe^{2+}. The prepared membranes were then washed and stored in pure ethanol in a cold room (4 °C) for further use.

2.4. PCB 126 dechlorination using Pd-Fe nanoparticles

To assess the reactivity of immobilized Pd-Fe NPs in membranes, PCB 126 was taken as a model compound. Dechlorination experiments were conducted in both batch mode and

convective flow mode. For batch experiments, 20 mL EPA glass vials were used. During the sub-sequent experiments the vials were placed on a shaker (250 rpm) to assure that all the PCB 126 can access the Pd-Fe NPs sites. Functionalized Pd-Fe-PAA-PVDF membranes (surface area of 17.3 cm^2 each) were then placed in vials (~ 15 μM PCB 126, $V_{ethanol}/V_{water}$ = 1/9, pH = 5.5–5.6). The experiment was terminated by removing 10 mL of organic solution from vials at different time intervals. To extract the organic compounds from both the solution and membrane phases, 10 mL of hexanes was poured into the previously extracted 10 mL of organic solution (Vorganic solution/Vhexanes = 1/1). 10 μL of 1000 ppm naphthalene_d8 was then added as an internal standard. After 1–2 h of shaking, the hexane phase was further analyzed using GC-MS. For conducting the convective flow study, a Pd-Fe-PAA-PVDF membrane was placed into a dead-end filtration cell. Here, the effective exposed membrane surface area is 13.2 cm^2. Then 30–50 mL of PCB 126 solution (~ 15 μM) was passed through the membrane under N_2 pressure. Permeate was collected after 8–10 min, when the reaction was observed to approach a steady state. Samples were collected at 10 min intervals while varying the operating pressure (1.36–4.76 bar). The collected samples were then extracted in hexanes before being analyzed by the GC-MS following the same procedure mentioned earlier.

2.5. Materials characterization

To evaluate the successful polymerization of the PAA in the pores of the PVDF membranes, the functionalized membranes were characterized using TGA, ATR-FTIR, SEM, contact angle measurements, surface zeta potential measurement, and water permeability studies. Thermogravimetric analysis (TGA) was conducted to study the mass loss and thermal stability of pore-modified PAA-PVDF membrane using TGA Q50 analyzer (TA Instruments, USA). Sample sizes ranged from 4 to 12 mg. The scanning temperature range was from room temperature up to 750 °C with a heating rate of 10 °C/min under N_2 atmosphere. The results were then analyzed using "TA Universal Analysis" software. Attenuated total reflectance Fourier transform infrared spectroscopy (ATR-FTIR, Varian 7000e) was used to examine the presence of functional groups in functionalized PVDF membranes. The samples were then placed on a diamond crystal, and the spectrum was evaluated between 500 and 4000 cm^{-1}, averaging 32 scans at a resolution of 4 cm^{-1}. Surface morphology of the functionalized membrane was studied using a scanning electron microscope (SEM, Hitachi S-4300). The membrane pore size and surface porosity (ratio of the pore area to the total membrane area) were analyzed using ImageJ software. The contact angles for both the bare and functionalized PVDF membranes were measured using a Krüss Drop Shape Analyzer instrument (DSA100). Zeta potential was analyzed using an Anton-Paar SurPASS electro-kinetic analyzer to characterize the membrane surface charge. Water permeability of the bare and functionalized PVDF membranes were performed using a laboratory-scale stainless steel pressure cell (Sepa ST, GE Osmonics, effective membrane area 13.2 cm^2) in dead-end mode [39].

The solution phase Pd-Fe nanoparticles were characterized by X-ray diffractometer (XRD) (Siemens D500) with Cu Kα (1.5418 Å) radiation (generator voltage of 40 keV, tube current of 30 mA). Inductively coupled plasma optical emission spectroscopy (ICP-OES, VARIAN VISTA-PRO) was used to quantify the concentration of Na and Fe ions in solution, after

acidification with nitric acid (1 v/v%). The amount of absorbed Fe in the functionalized membranes during the ion exchange process was then determined by mass balance. The composition of the top layer of Pd-Fe-PAA-PVDF membrane was performed using X-ray photoelectron spectroscopy (XPS) (K-alpha, Thermo-Scientific) with aluminum anode. The measurement of NP size and distribution was conducted both on surface and inside the Pd-Fe-PAA-PVDF membrane pores after preparing a lamella using a FIB-SEM (FEI Helios Nanolab 660) instrument. A transmission electron microscopy (TEM, JEOL 2010F) coupled with energy dispersive x-ray spectroscopy (EDS) and an electron energy loss spectroscopy (EELS) were also used to observe the NP distribution inside Pd-Fe-PAA-PVDF membrane layer. Line scan and elemental mapping were conducted using a scanning transmission electron microscopy (STEM) mode.

Finally, while performing degradation studies using the Pd-Fe-PAA-PVDF membranes (both in batch and convective flow mode), the concentrations of produced biphenyl and the remaining PCB 126 were calculated using a coupled gas chromatography (Varian CP-3800)-mass spectrometry (Saturn 2200) instrument with helium as carrier gas.

3. Results and discussion

3.1. Mass gain of functionalized membranes

The effective polymerization of PAA in the pores of PVDF membranes could be calculated by measuring the difference of weight change of membranes before and after functionalization. In Fig. 2a, the average mass gain for all the six batches (each with a different matrix of monomer (M) and cross-linker (X) concentrations) are represented in a bar chart. It is clear from Fig. 2a that when 10 wt% of the monomer concentration was used during functionalization as in Batches A, B and C, the observed average mass gain was 4–5% despite of using different concentrations of cross-linker (0.5–2 mol%). Whereas, when 20 wt% of monomer concentration was used as in Batches D, E and F, these results have an average mass gain of around 15–16%. This mass gain data is consistent with our previous reported works [34,38,40].

To know the maximum mass gain, a bare PVDF membrane was soaked in DIUF water for 30 min. It was found a maximum mass gain of 21–23 wt% (showed with a green dotted line in Fig. 2a). The maximum mass gain results reveal that values of mass gain of the different batches (A to F) of membrane are within the range. For a base porosity of 40%, functionalization of a PVDF membrane using a 10 wt% polymer solution allows the membrane to retain porosity around 30–31%, while when using a 20 wt% of polymer solution, the membrane is only able to retain a porosity between 9% and 12% as shown in Fig. 2a. It is interesting to note that changing the concentration of the cross-linker does not affect the mass gain of the functionalized membrane, which is reasonable since X concentration is much lower compared to M concentration and it is used mainly to deter entanglement of polymer chains during the polymerization reaction. This is also confirmed by a factorial and response surface design analysis mentioned at the end of this document. One of the earliest researchers to report on the effect of cross-linking on the physical properties of polymers was Nielsen [41]. Later, Kjøniksen et al. and Zhao et al., reported the effect of cross-linking density on the rheology and its mechanical properties in different

aspects [42,43]. However, none of them discussed the effect of cross-linkers on mass gain during polymerization reaction. It is also observable from Fig. 2a that mass gain increased three-fold when the monomer concentration was changed from 10 wt% to 20 wt%, despites of different cross-linker concentration.

The mass gain profile of modified PAA-PVDF membrane was further investigated by the TG analysis. In Fig. 2b the TG analysis thermograms for bare PVDF membrane (blue line), 10 wt% PAA-PVDF membrane (black big dashed line), 20 wt% PAA-PVDF membrane (pink small dashed line) and PAA powder (red line) are shown. The TG analysis can provide information on PAA content, PAA decomposing temperature and membrane thermal stability by observing the minute weight change of the sample with temperature. The bare PVDF membrane shows only one-step sharp weight loss around 420–440 °C, which corresponds to the degradation of the CF_2 chain [44,45]. The PAA powder also shows one step wide weight loss in the temperature range 215–490 °C. However, the PAA-PVDF membrane (-COOH form) exhibits a distinct three-step degradation process. The first slight weight loss is around temperature range of 215–310 °C due to the formation of anhydride [46,47]. The second weight loss is observed at the temperature range from 310–485 °C, corresponding to further decomposition of polyacrylic anhydride [46,47]. The final weight loss occurs at 485 °C, which is attributed to the decomposition of the PVDF side chains. From Fig. 2b, it is clear that with an increase of PAA content in PVDF membrane the thermograms are shifted towards the thermograms of PAA. This confirms difference in weight of the modified PAA-PVDF membrane due to difference in loading of PAA in bare PVDF membrane.

3.2. ATR FT-IR spectra and SEM image analysis

The ATR FT-IR spectra of the bare and functionalized PVDF membranes shown in Fig. 3 confirm the resulting in situ polymerization inside membrane pores. The absorption peaks characteristic of fluorocarbon groups (-CF_2-) of the PVDF chains lie in the region of 950–1220 cm^{-1}, as expected are clearly visible in Fig. 3a (blue line) [48]. The appearance of peaks around 1700 cm^{-1} and 1550 cm^{-1} in Fig. 3b (green line) is due to carbonyl stretch and antisymmetric stretching of carboxyl groups (-COOH), respectively, of the polyacrylic acid polymer [49]. In addition, the broad peak in Fig. 3b between 2700 and 3400 cm^{-1} is demonstrating the presence of O–H group from the synthesized polymer [34]. Together, these results demonstrate the successful polymerization of PAA in PVDF membrane matrix.

Surface morphologies of the PVDF and PAA functionalized PVDF membranes were characterized by SEM as shown in Fig. 3. The bare PVDF membrane (Fig. 3c) shows a porous structure with an average pore size of 262 ± 60 nm. The polyester backing of the bare PVDF membrane is clearly visible in Fig. 3d. The diameter and morphology of the membrane pores decreased substantially after the PAA polymerization reaction, becoming uniformly circular and smaller with an average pore size of 65 ± 7 nm (Fig. 3e); which conform with our earlier reported works [35,40]. The pores of the functionalized PVDF membrane reduced in size due to formation of PAA domain inside the pores.

3.3. Contact angle measurement and surface zeta potential analysis

Contact angles (water, pH ~ 5.5) of the bare and functionalized PVDF membrane were measured to assess any change in the hydrophilicity of the modified layer. The contact angle decreased from 79.96° (± 3.86°) to 55.90° (± 0.06°), indicating the membrane became more hydrophilic upon functionalization with PAA polymer. A sessile drop method was used to measure the contact angle of bare PVDF membrane. However, for hydrophilic surfaces it is difficult to measure the contact angle by sessile drop method due to: i) high surface free energy that causes water droplet to spread rapidly, and ii) fast absorption of water by PAA hydrogel [50]. To overcome those limitations, a captive bubble method was used for functionalized PAA-PVDF membrane [51,52].

The surface zeta potential of the bare PVDF and the functionalized PVDF membranes were compared to study the change in surface charge. Fig. S1 shows the comparison of the pH dependence of the zeta potential for blank PVDF membrane (green line) to that of functionalized PAA-PVDF membrane (red line). The blank PVDF membrane is showing overall negative change distribution on the surface. The blue line in the graph is representing the commercial hydrophilized PVDF membrane confirming the same trend of surface charge distribution as functionalized PAA-PVDF membrane. The PAA-functionalized membrane shows a phase transition (isoelectric point) near pH ~ 2.6, which is attributed to the pKa value of carboxyl groups present in PAA [35,53,54]. A change in surface charge confirms the presence of PAA layer in functionalized PVDF membrane.

3.4. Water permeability studies of pH responsive functionalized membrane

To determine the pH response of the PAA functionalized membrane and the effects of monomer (M) and cross-linker (X) concentrations on its permeability, water flux tests were performed on six different batches (mentioned in Table 1) of membranes. The role of pH in the responsive behavior of the PAA functionalized membranes is thoroughly documented in literature [8,55,56]. The water permeability of the bare PVDF membrane was found around 6250 L m^{-2} h^{-1} bar^{-1} (LMH/bar) at pH 4. However, the permeability dropped substantially after functionalization making the membrane pH responsive. This responsive behavior of PAA-PVDF membrane allows the water permeability to be changed in response to different pH environments. In Fig. 4 the effects of pH on the water permeability of the PAA-PVDF functionalized membrane are shown. PAA hydrogel can swell or shrink by tuning its protonation state and the molar mass of the solution [55]. At high pH, PAA swells, resulting in a decrease in the effective pore size and water permeability. On the contrary, when the permeate pH is decreased, the polymer chain shrinks and the pores return to their original size, thereby increasing water permeability.

The permeability of the membranes shown in Fig. 4 decreased with increasing pH, confirming the successful PAA functionalization within the PVDF pores. This behavior of membrane water permeability is consistent with previous findings [35,39,56]. In Fig. 4a the water permeability of batch C (M = 10 wt%, X = 2 mol%) is provided. The water permeability with a different pH in Fig. 4a can be fitted (continuous line in Fig. 4a) with the Eq. (1) to obtain the pKa value [56]. The resulting pKa value is 5.8 for batch C, where, $A_{,max}$ = 116 LMH/bar (low pH) and $A_{,min}$ = 59 LMH/bar (high pH). In Eq. (1), A is the

membrane water permeability in LMH/bar. Similarly, the water permeability data of batch F (M = 20 wt%, X = 2 mol%) with different pH (as shown in Fig. 4b) can also fitted (continuous line in Fig. 4b) with Eq. (1). In this case the value of pKa is 6. Here, $A_{,max}$ = 2.75 LMH/bar (low pH) and $A_{,min}$ = 0.4 LMH/bar (high pH). It is worth mentioning that, while increasing the monomer concentration (M) from 10 to 20 wt% while keeping the cross-linker concentration (X) constant at 2 mol%, the water permeability drops about 42 times at low pH (4) and around 147 times at high pH (8.5). This change in water permeability pattern for varying M and X confirms the quantitative measurement of responsive behavior of PAA-PVDF membrane. The subsequent results of water flux study with different values of pH for other batches of functionalized membranes are provided in Fig. S2.

$$A = \left\{ A_{max}{}^{1/2} - \frac{[COO^-]}{[COOH] + [COO^-]} \left(A_{max}{}^{1/2} - A_{min}{}^{1/2} \right) \right\}^2 \quad (1)$$

where,

$$\frac{[COO^-]}{[COOH] + [COO^-]} = \frac{1}{1 + 10^{(pKa - pH)}}$$

Permeability data of six different batches of functionalized membranes at pH 4 and 8.5 are presented in Fig. 5. It is observable that with an increasing M and X concentrations, the permeability of water through the membrane decreases. This allows a wide range of variation of responsive behavior of PAA functionalized membranes in quantified terms of water permeability that ranges from 270 to 1 LMH/bar, by altering M (10–20 wt%) and X (0.5–2 mol%) concentrations. Permeability data at two different pH (4 and 8.5) widely varies, while M is 10 wt%. But it does not vary in the same range when the M is 20 wt%. Another interesting finding is that with 20 wt% monomer concentration, the flux remains constant for a pH 4 and a pH of 8.5 when the cross-linker concentration is increased from 1 to 2 mol% (Batch E and F in Fig. 5). Further addition of a cross-linker will not affect swelling property of the functionalized membrane anymore, resulting in a fixed of permeability. This is due to high entanglement of polymeric chains inside the PAA-PVDF membrane pores resulting hindrance for charge neutral carboxyl groups for chain expansion and contraction. This explains why the swelling of the PAA resulted in a saturated pore domain with 1 mol% of cross-linker, sufficient to keep the monomer chains apart and reduce the entanglement of polymer chain in membrane pores. Fig. 5 confirms that the response behavior of PAA-PVDF membrane varies significantly in terms of difference in water permeability between low and high pH when monomer concentration is low (10 wt%). However, it does not vary in the same extent when the monomer concentration is in the high end (20 wt%).

3.5. Pd-Fe nanoparticle loading and particle size distribution

Before immobilization of nZVI in the pore matrix of the functionalized PAA-PVDF membrane, iron NPs in solution phase were prepared by dissolving $FeCl_2$ salt in

deoxygenated water (pH 5.5–5.7). Afterwards, the addition of $NaBH_4$ in the solution was used to reduce the Fe^{2+} to Fe^0. From TEM images of Fig. S3a–c, we can see all the NPs diameters are in the range of 5–33 nm. In addition, HRTEM images in Fig. S3d confirms formation of amorphous Fe structures together with iron oxides on the edges which is consistent with the literature [57–60]. Further, peaks from the EDS spectrum in Fig. S4 confirm the formation of Fe NPs in the solution phase. The Pd-Fe NPs are prepared in solution phase are analyzed by XRD. The crystalline structure of Pd, and Fe were analyzed and confirmed through comparison with XRD patterns published in the literature [40]. In Fig. S5, the XRD pattern of crystalline phases of bimetallic Pd-Fe nanoparticles were demonstrated. Based on the dominant peak and using Scherrer formula the particle size could be measured [61]. In this case the metallic $Fe_{[110]}$ is the dominant peak and corresponding particle size was calculated is around 16 nm, which falls in the limit of nanoparticle size we have mentioned earlier based on corresponding TEM data. After synthesis and characterization of the solution phase Pd-Fe NPs, we successfully immobilized the Fe and Pd NPs in the PAA-PVDF membranes pore domain following the method mentioned earlier. Fig. S6 shows a typical FIB-SEM image which confirms a homogeneous immobilization of NPs in Pd-Fe-PAA-PVDF membrane surface.

To ensure that Fe^{2+} is immobilized in the PAA network of the functionalized membrane and does not precipitate out of the membrane pores, we monitored the release of the cation displaced by Fe^{2+} during ion exchange. For this reason and to prevent pH drop during Fe^{2+} capture, PAA-PVDF membranes were first ion exchanged with Na^+ (Na^+-PAA-PVDF). There was no evidence of iron precipitation during immobilization, and no leaching of iron from the membrane was detected during the experiments. In Fig. 6a, it is demonstrated that the amount of Fe loading in mg/cm^2 surface area (0.225 cm^3 volume) of Fe-PAA-PVDF membrane is a function of different combinations of monomer (M) and cross-linker (X) concentrations. The amount of Fe loading varied from 2.83 to 12.4 mg per mentioned surface area which is equivalent of 0.21–0.94 mg/cm^2 of membrane surface area. The difference of loading is due to variation of available carboxyl groups in the membrane pore domain. The Loading was minimum when M and X concentrations were minimum (10 wt% and 0.5 mol%, respectively), which proves the presence of less carboxyl groups during the functionalization of membrane. On average, the Fe loading was found to be in the range of 6.5–8 mg with the same specific volume for most of the combinations of monomer and cross-linker densities. This means that variation of M and X does not confirm variation of the available carboxyl group in the membrane domain to perform double ion exchanges for in-situ synthesize Fe NPs in the membrane.

However, Fe loading is maximized to a value of 12.4 mg in the same surface volume, when M and X densities are 20 wt% and 1 mol% respectively. This suggests that a specific combination of M and X reveal a maximum amount of deprotonated carboxyl groups in the PAA chains in PVDF membrane in order to capture Fe^{2+} during ion exchange. In contrast, a slight increase in cross-linker concentration as in batch F (M:20 wt% & X:2%) resulted in a lower loading (6.49 mg) of Fe (see Fig. 6a). This is due to the fact that a higher concentration of cross-linker results in an increase in the entanglement of the PAA chains in membrane domain, hindering the ability of the carboxyl groups to be involved in ion exchange. Such higher concentration also cause some of the swollen gel to come out of

pores and lose the stability of the PAA gel [39]. The permeability data during the Fe^{2+} ion exchange experiments are shown on the right y-axis of Fig. 6a. Interestingly during Fe^{+2} ion exchange the water permeability of membrane increases slightly compare to that of PAA-PVDF membrane due to overall charge positivity of membrane, especially when the monomer concentration is 10 wt%. However, this observation is not so prominent when monomer concentration is 20 wt%, indicating that at higher concentration of monomer and cross-linker the PAA-PVDF membrane is losing its responsive nature in course of Fe^{2+} loading. The most interesting aspect of responsive nature of PAA-PVDF membrane is, it is always possible to restore responsive nature by dislodging the NPs if there is any significant loss of reactivity performance of NPs. This attribute makes it suitable for long time usage. After the Fe NPs are synthesized by reduction with $NaBH_4$, solution of K_2PdCl_4 solution (Pd as 1 wt% of Fe) was passed through Fe-PAA-PVDF membrane reducing Pd^{2+} to Pd° for all the batches of membrane.

In order to understand the impact of variation of monomer and cross-linker concentrations on the metallic NP size distribution during ion exchange process, the size distribution of NPs was measured on the surface and inside the membrane pores after the immobilization of the Pd-Fe NPs. PAA acted as a stabilizer of the Fe precursor in the NP synthesis. It also able to control the particle size depending on the available proximity distance between polymer chains. Both the rates of nucleation and particle growth could be retarded in presence of PAA in functionalized membrane pores [11,62]. In Fig. 6b we have shown the variation of the Pd-Fe particle size distribution for different batches of Pd-Fe-PAA-PVDF membranes in a bar chart. At the top of all blue bars in Fig. 6b, we put the average value of particle size with their standard error of the mean. The average particle size varies from 16 to 23 nm, which agrees with available reported data [63]. However, around 68–87% of NPs fall in the range of 10–25 nm for different combinations of M and X. In Fig. 6b, it is also shown that when the X concentration increases while the M concentration is kept the same, the percentage of smaller particles (green bars) has increased and vice versa (red bars). This implies that by tuning the cross-linker concentration during the polymerization reaction it is possible to get much smaller particles by in-situ synthesis.

The XPS analysis results shown in Fig. 7 was performed to study the surface composition of Pd-Fe-PAA-PVDF membrane. The XPS survey scan (Fig. 7a) shows the presence of Pd° and Fe° over the top surface of the membrane. In addition of Pd and Fe peaks, the other observed peaks are for the elements C, N, O, F and Na. The C 1s peak at binding energy of 289 eV is due to the presence of carbon in PVDF, AA and cross-linker MBA. The N 1s peak at binding energy of 402 eV is for N as amide ($-NH_2$) in cross-linker MBA. The O 1s peak at binding energy of 534 eV is due to the presence of O in carboxyl groups (-COOH). The F 1s peak at binding energy of 691 eV is for F which is present in fluorocarbon groups ($-CF_2-$) of PVDF. A small peak of Na 1s was observed around binding energy of 1074 eV due to presence of some Na while reducing Fe^{2+} to Fe° and Pd^{2+} to Pd° using sodium borohydride. The distinct doublet peaks for Fe 2p which are observed at binding energies of 713 and 727 eV are assigned for Fe $2p_{3/2}$ and Fe $2p_{1/2}$ are due to presence of Fe° which is clearly shown in Fig. 7b [64]. Apart from that Fe 3p and Fe 3s peaks are observed at the binding energies of 60 and 98 eV respectively depicted in survey scan in Fig. 7a. Two doublet peaks at binding

energies of 338 and 343 eV are attributed to Pd $3d_{5/2}$ and Pd $3d_{3/2}$, associated with Pd° that was deposited on top of Fe NPs shown in Fig. 7c [64].

Immobilization, size and morphology of the Pd-Fe NPs inside the pores at various depths were measured using FIB-SEM as shown in Fig. 8. Some aggregations of Pd-Fe NPs were observed in surface (Fig. S6) but fewer aggregates and more homogeneity of the Pd-Fe NPs were observed inside the pores as shown in Fig. 8. At a depth of 3.196 μm from the top surface we can see (Fig. 8a) all Pd-Fe NPs are well immobilized on the wall of the pores. For another membrane with different combinations of M and X, we also observe (Fig. 8b) the even distribution of Pd-Fe NPs inside the pore. However, due to a smaller distance (500 nm) from the top surface, few aggregations of NPs were detected. This explains why with the increase of the distance from the top surface the Pd-Fe NPs are uniformly immobilized. In Fig. 8c a zoomed image of the square box in Fig. 8a is shown, which confirms that most of the Pd-Fe NPs are circular in nature. It is very interesting to find out that particle size inside the pores are smaller (9–14 nm) in size than those on the surface (16–23 nm) as well as more uniformly dispersed in pore wall. To explain this phenomenon during immobilization of Pd-Fe NPs, PAA-PVDF membrane has been exposed to a constant pressure gradient throughout convective flow mode ion exchange process. This overcomes the mass transfer limitation during immobilization process resulting less agglomeration of NPs, well dispersion of NPs inside pore domain ultimately creating smaller NPs inside [65]. However, on the surface the initial immobilized NPs are exposed continuously exposed in order to make more clusters of Pd-Fe NPs resulting relatively bigger NPs.

Finally, the inner surface of the membrane was characterized by TEM, high resolution TEM and selected area electron diffraction (SAED) as shown in Fig. 9. A typical TEM image of the inside surface of Pd-Fe-PAA-PVDF membrane is shown in Fig. 9a, where one can distinctly see the dispersion of Pd and Fe NPs. The light grey areas are Fe NPs and the darker ones are Pd NPs, further confirmed by a single point scanning transmission electron microscopy (STEM) and point EDS shown in Fig. S7. It is also clear from Fig. 9a that, most of the Pd NPs are deposited on the surface of the Fe NPs, and not over the carbon polymer layer. The EDS spectrum taken in the same area shown in Fig. 9b, demonstrates the presence of Pd and Fe peaks. In Fig. 9c SAED pattern displays a diffraction halo (representing core carbon of the polymer) and multiple diffraction rings, representing different phases of Pd and Fe elements which agrees with literature [19,60]. All these characterizations by TEM were conducted by removing a thin lamella of membrane from the inside of the membrane with the help of FIB depicted in Fig. 9d. Lastly, line scanning of the inner surface performed in STEM mode (Fig. 9e) further reveals a uniform distribution of Pd and Fe elements (Fig. 9f) inside the Pd-Fe-PAA-PVDF membrane. In addition of detail characterization of the Pd-Fe-PAA-PVDF membrane with TEM, the elemental mapping inside of the functionalized membrane was performed using FIB. Fig. S8 demonstrates the elemental mapping of the Pd-Fe-PAA-PVDF membrane. The Pd and Fe are well incorporated inside the pore domain of PAA-PVDF membrane which is clear from Fig. S8. The corresponding EDS analysis in the same area of the lamella shows the atomic distribution of Pd and Fe elements inside functionalized Pd-Fe-PAA-PVDF membrane shown in Fig. S9.

3.6. PCB 126 degradation study in batch mode, convective flow mode and kinetics study

Immobilized Pd-Fe NPs on polymer domain of functionalized PAA-PVDF membrane offers an opportunity to study the dechlorination of PCB 126. Bimetallic Pd-Fe NPs have been extensively used for degradation of chlorinated organics for their superior catalytic activity [15,16,25,26,66]. However, mass transfer during dechlorination in Pd-Fe-PAA-PVDF membrane platform could be critical due to its dependence on membrane pore size, porosity, Pd-Fe NPs loading, available reaction surface area, channeling and finally, fluid mixing during reaction. To address most of these issues, PCB 126 degradation in batch and convective flow modes were studied. Initially, solution phase dechlorination experiment was conducted. In this case, almost all the PCB 126 was converted to biphenyl within 4 h, as shown in Fig. S10.

The dechlorination results from batch studies are shown in Fig. 10a. A control experiment was performed to address the evaporation of the reactant. The rate of PCB 126 degradation varies with the different amount of Fe loading for different batches of membrane. From Fig. 10a we see PCB 126 concentration reduces to 40%, while the Fe loading is 2.83 mg; whereas, it reduces to almost zero when the Fe loading is 12.4 mg, in a same time scale of 4.5 h. This suggests, it is possible to tune the dechlorination of PCB in same membrane surface domain, by manipulating the Fe loading. To explain this phenomenon, it is well documented that in presence of water Fe acts as electron source in corrosion mechanism [25]. It continuously converting from Fe° to Fe^{2+} making H_2 gas and OH^- radical. In presence of Pd, H_2 is quickly converted to H· radical, which ultimately enhance the dichlorination reaction. The degree of surface Pd loading is proportional to the initial amount of Pd [25,67]. However, more Fe loading offers more Pd to do ion exchange and attach onto the Fe shell during ion exchange process. This ultimately creates more reactive Pd-Fe NPs surfaces available for dechlorination reaction in the membrane pore domain, proportional to the initial Fe loading. The maximum yield of biphenyl in the experiment was found around 63%, which defers from theoretical estimation. This deviation of mass balance is also reported in available literature [40,68]. Formation of PCB intermediates, adsorption of some biphenyl in hydrophilic membrane, and further degradation of biphenyl might account for this deviation [40]. However, investigations have shown that catalytic hydro-dechlorination by Pd usually leads to the formation of a small amount of chlorinated intermediates, likely to be attributed to complete dissociation of carbon-chlorine bonds at the Pd surface [25].

PCB 126 dechlorination by Pd-Fe NPs follows a pseudo-first order rate law during batch study experiments following Eq. (2) [25]:

$$r = -\frac{dC}{dt} = -\mathrm{K_{obs}}C = -K_{sa}\rho_m a_s C \quad (2)$$

where, r is the reaction rate (mol L^{-1} h^{-1}), C is concentration of PCB 126 (mol L^{-1}) at reaction time, t (h), K_{obs} is the observed rate constant (h^{-1}), K_{sa} is surface-area normalized rate constant (L m^{-2} h^{-1}), ρm is the nanoparticle loading density (g L^{-1}), and a_s is the specific surface area of Pd-Fe NPs immobilized in membrane (m^2 g^{-1}). In Fig. 10b we have

shown the variation of observed reaction rate K_{obs} (h^{-1}) with loading (mg) of Fe in membrane domain. The observed reaction rate, K_{obs} (h^{-1}) varies linearly from the value of 0.22–1.35 (h^{-1}) with the amount of Fe loading from 2.83 to 12.4 mg for different batches of membrane. This means for per mg of catalyst loading in Pd-Fe-PAAPVDF membrane the observed batch reaction rate (K_{obs}) for PCB 126 degradation is 0.08–0.1 h^{-1}. On the right y-axis of Fig. 10b data for surface normalized reaction rate, K_{sa} (L m^{-2} h^{-1}) is given, which varies from 0.033 to 0.054 (L m^{-2} h^{-1}). Dechlorination of PCB 126 is a surface mediated reaction, which usually involves several steps in the overall reaction including the diffusion of reactant PCB 126 to the surface, a chemical reaction on the surface, and the diffusion of a product biphenyl back into the solution [25]. For the variation of Fe loading from 2.83 mg to 12.4 mg in membrane pores, the loading densities (ρm) varied from 0.145 to 0.62 (g L^{-1}). The specific surface area (a_s), also a function of Pd-Fe NPs diameter varied from 33 to 48 (m^2 g^{-1}) when the NPs diameters varied from 16 to 23 nm. As K_{sa} is a function of nanoparticle loading density (ρm) and specific surface area (a_s), it did not vary that much due to small variation of average Pd-Fe NPs diameter. However, the magnitude of variation results due to the difference in iron loading that is for loading density (ρm). Fig. 10b shows that when the Fe loading is increased during the ion exchange experiment, the available Pd-Fe core shell structures also increase proportionately creating more surface area for degradation reaction.

To understand the kinetics of PCB dechlorination in a convective flow mode, Pd-Fe particles are regarded to be uniformly distributed in the assumed cylindrical pores inside the membrane. A laminar flow reactor (LFR) model could be perceived in this cylindrical pore due to the small Reynolds number (Re < < 1) [69,70]. For laminar flow in each cylindrical pore, the flow profile is described by Eq. (3) [69]:

$$u(r) = 2u_0\left(1 - \frac{r}{R}\right)^2 \quad (3)$$

where, R is the pore size of the functionalized membrane. u_0 and $u(r)$ are the velocities at center and radius r, respectively.

Due to the large Peclet number (10^2–10^3) in this study, the mass diffusion term can be neglected from the general convection-diffusion equation. In addition, $u(r)$ is only related to pore radius. The convective-diffusion equation (at steady state) can be simplified and integrated as a function of pore axial distance shown in Eq. (4):

$$C(r, \quad z) = C(r, \quad 0)\exp\left[-\frac{K_{obs}z}{u(r)}\right] \quad (4)$$

A cross-section averaging method was used to integrate the concentration over the radial dimension to obtain the mean concentration $\bar{C}$ at certain axial distance z [69,70]. The mean outlet concentration $\bar{C}_{final}$ (z = membrane thickness) can be calculated using Eq. (5) [69]:

$$\bar{C}_{final} = \frac{\int_0^r C(r,z)u(r)2\pi r dr}{\int_0^r u(r)2\pi r dr} \quad (5)$$

This equation can be used to fit K_{obs} values from experimental reaction data (τ, $\bar{C}_{initial}$, $\bar{C}_{final}$). Matlab was used to find the most fitted K_{obs}. The Pd-Fe-PAA-PVDF membrane used in convective flow dechlorination was with maximum amount of Fe loading (12.4 mg/13.2 cm^2 membrane surface area). The permeability during degradation study for this membrane was found around 1.33 LMH/bar. The residence time (τ) was varied by changing applied cell pressure from 8.16 to 11.56 bar. For residence times of 5.15 s, 11.2 s, 27.17 s and 46.2 s, the corresponding dichlorination percentages of PCB 126 were found to be 84%, 93%, 98% and 98.6%, respectively as shown in Fig. 10c. In this experiment, we also ran a PCB 126 solution through a Fe-PAA-PVDF membrane as a control so as to detect any possible interference of nZVI. The fitted K_{obs} value was found to be 0.452 s^{-1}. If the membrane is considered a plug flow reactor (PFR) the corresponding K_{obs} is found to be 0.09 s^{-1}. However, if the membrane is assumed to be a continuous stirred-tank reactor (CSTR) the K_{obs} is obtained to be 1.38 s^{-1}. The calculated K_{sa} (L m^{-2} h^{-1}) for convective flow mode degradation in membrane platform was calculated from K_{obs} (0.452 s^{-1}) data. The value of K_{sa} is 0.113 L m^{-2} h^{-1} which is 2.13 times higher than K_{sa} of batch degradation results, suggesting degradation of PCB 126 in a convective flow mode eliminates the effect of diffusion resistance.

3.7. Statistical analysis between input (monomer and cross-Linker) and response variables

A two-way factorial design with repetitions was performed in order to determine whether the M and X concentrations significantly affected the response variables. To perform statistical analysis, it has been considered M has three levels (0, 10 and 20 wt%) and X has four levels (0, 0.5, 1.0 and 2.0 mol%). Although numerous responses resulting from these combinations of M and X can be analyzed, such as the NP size or the rate of reaction; however, these responses are affected mainly by two main responses: i) the amount of PAA present within the functionalized membranes (mass gain) and ii) the permeability (A). Permeability was considered because it is a dynamic response on the actual separation/reaction process on PAA-PVDF membrane platform, unlike the static mass gain. As the permeability changes with pH, the response analyzed is the ratio between permeability values at high pH and at low pH (A_{min}/A_{max}). The change in responsiveness factor (A_{min}/A_{max}) could affect ion exchange process, hence affecting Fe loading, NP size and, dechlorination performance. The present analysis was performed with 95% confidence in all cases.

A response surface design was selected to better understand the response results. This methodology was used to refine the models after determination of the factorial design analysis (See Section S1) and helps to detect curvatures in the response surfaces. The Interaction effects and main effects (individual effects) of the concentrations of M and X on

mass gain (%) and responsive factor (A_{min}/A_{max}) are shown in Figs S11 and S12. In Fig. 11 the raw response surfaces (in color scale) and the fitted values (contours) are shown as a function of M and X. The effects of M and X concentrations are increasing for mass gain, but decreasing for the responsiveness (A_{min}/A_{max}). The regression equations for each response surface are shown in Section S2.

As mentioned in the factorial design analysis (Section S1), the effect of X is not significant above 1.0 mol% for almost all mass gain values. The value of mass gain increases only where X is higher than about 1.8 mol% and M is higher than 15 wt%. As expected, mass gain increases with an increase in M for all cases as depicted in Fig. 11a. However, the responsiveness (A_{min}/A_{max}) decreases with an increase of M (Fig. 11b). Since more PAA is in the membranes at higher M, the swelling is larger at higher pH. However, when $X \leq 0.5$, A_{min}/A_{max} does not change significantly due to fewer polymer entanglements, decreasing the swelling capacity of the cross-linked PAA. It is worth mentioning that these statistical analyses between input variables (M and X) to response variables only work for the type of membrane selected for these experiments and any changes in the membrane support (pore size, thickness, etc.) will affect the responses. However, the discussed procedure related to the parameters of the examined membrane can be extended to other membrane types as well.

4. Conclusions

This paper demonstrates quantitatively the effect of monomer and cross-linker concentration during the functionalization of pH responsive membrane on mass gain, water permeability, Pd-Fe NPs loading, and the degradation of PCB 126. The results obtained during this study confirm quantitative tuning of the responsive behavior of membrane in terms of water permeability, NPs size, metal loading and rate of PCB 126 degradation by varying monomer and cross-linker concentration. Degradation study in convective flow mode through Pd-Fe-PAA-PVDF membrane platform shows 98.6% PCB 126 is degraded at a residence time of 46.2 s. Based on surface normalized reaction rate data for PCB 126 dechlorination, a convective flow through mode reveals a much faster degradation due to overcoming the mass transfer limitation. Details of Pd-Fe-PAA-PVDF membranes surface and pores as well as size, shape and size-distribution of Pd-Fe nanoparticles have been established by using different characterization tools such as TGA, contact angle measurement, surface zeta potential, XRD, SEM, XPS, FIB, TEM and other methodologies. Later, statistical analysis of interaction between inputs (monomer, cross-linker) and response variables (mass gain, permeability ratio) show that statistically significant interaction exists between monomer and cross-linker concentration. Further statistical depiction of the responsive behavior of PAA-PVDF membrane suggests that practical application for water remediation can be reasonably anticipated.

Supplementary Material

Refer to Web version on PubMed Central for supplementary material.

Acknowledgements

This research is primarily supported by the NIH-NIEHS-SRC (Award number: P42ES007380). Partial support is also provided by NSF KY EPSCoR program (Grant number: 1355438). We thank John May and Megan Combs of Environmental Research and Training Laboratory (ERTL), University of Kentucky for GC-MS and ICP-OES analytical assistance. We also thank Dr. Dali Qian and Dr. Nicolas Briot of Electron Microscopy Center, University of Kentucky for extensive support to prepare samples for TEM and FIB instruments as well as to analyze TEM and FIB samples. Finally, we thank Matthew K. Defrese and Dr. Patrick J. Marsac, College of Pharmacy, University of Kentucky for helping us to conduct TG analysis in their laboratory.

Abbreviations:

PVDF	polyvinylidene difluoride
PAA	polyacrylic acid
KPS	potassium persulfate
MBA, N	N'- methylenebisacrylamide
PCB 126	3,3',4,4',5-pentachlorobiphenyl
LMH	L/m^2-h
DIUF water	deionized ultra-filtered water
M	monomer
X	cross-linker

References

[1]. Werber JR, Osuji CO, Elimelech M, Materials for next-generation desalination and water purification membranes, Nat. Rev. Mater 1 (2016) 16018.

[2]. Shannon MA, Bohn PW, Elimelech M, Georgiadis JG, Marinas BJ, Mayes AM, Science and technology for water purification in the coming decades, Nature 452 (2008) 301–310. [PubMed: 18354474]

[3]. Elimelech M, Phillip WA, The future of seawater desalination: energy, technology, and the environment, Science 333 (2011) 712–717. [PubMed: 21817042]

[4]. Baker RW, Membrane Technology and Applications, John Wiley & Sons, West Sussex, United Kingdom, 2012.

[5]. Park HB, Kamcev J, Robeson LM, Elimelech M, Freeman BD, Maximizing the right stuff: the trade-off between membrane permeability and selectivity, Science 356 (2017).

[6]. Ulbricht M, Advanced functional polymer membranes, Polymer 47 (2006) 2217–2262.

[7]. Liu F, Urban MW, Recent advances and challenges in designing stimuli-responsive polymers, Prog. Polym. Sci 35 (2010) 3–23.

[8]. Bhattacharyya D, Schäfer T, Wickramasinghe S, Daunert S, Responsive Membranes and Materials, John Wiley & Sons, West Sussex, United Kingdom, 2012.

[9]. Xiao L, Isner A, Waldrop K, Saad A, Takigawa D, Bhattacharyya D, Development of bench and full-scale temperature and pH responsive functionalized PVDF membranes with tunable properties, J. Membr. Sci 457 (2014) 39–49.

[10]. Lewis SR, Datta S, Gui M, Coker EL, Huggins FE, Daunert S, Bachas L, Bhattacharyya D, Reactive nanostructured membranes for water purification, Proc. Natl. Acad. Sci. USA 108 (2011) 8577–8582. [PubMed: 21606340]

[11]. Xu J, Bhattacharyya D, Membrane-based bimetallic nanoparticles for environmental remediation: synthesis and reactive properties, Environ. Prog. Sustain. Energy 24 (2005) 358–366.

[12]. Han L, Qian L, Yan J, Chen M, Effects of the biochar aromaticity and molecular structures of the chlorinated organic compounds on the adsorption characteristics, Environ. Sci. Pollut. Res. Int 24 (2017) 5554–5565. [PubMed: 28032286]

[13]. Smuleac V, Varma R, Sikdar S, Bhattacharyya D, Green synthesis of Fe and Fe/Pd bimetallic nanoparticles in membranes for reductive degradation of chlorinated organics, J. Membr. Sci 379 (2011) 131–137.

[14]. Xin J, Tang F, Zheng X, Shao H, Kolditz O, Lu X, Distinct kinetics and mechanisms of mZVI particles aging in saline and fresh groundwater: H_2 evolution and surface passivation, Water Res. 100 (2016) 80–87. [PubMed: 27179595]

[15]. Zhao X, Liu W, Cai Z, Han B, Qian T, Zhao D, An overview of preparation and applications of stabilized zero-valent iron nanoparticles for soil and groundwater remediation, Water Res. 100 (2016) 245–266. [PubMed: 27206054]

[16]. Sun Y, Li J, Huang T, Guan X, The influences of iron characteristics, operating conditions and solution chemistry on contaminants removal by zero-valent iron: a review, Water Res. 100 (2016) 277–295. [PubMed: 27206056]

[17]. Crane RA, Scott TB, Nanoscale zero-valent iron: future prospects for an emerging water treatment technology, J. Hazard. Mater. 211–212 (2012) 112–125. [PubMed: 22305041]

[18]. O'Carroll D, Sleep B, Krol M, Boparai H, Kocur C, Nanoscale zero valent iron and bimetallic particles for contaminated site remediation, Adv. Water Resour 51 (2013) 104–122.

[19]. Yan W, Herzing AA, Kiely CJ, Zhang WX, Nanoscale zero-valent iron (nZVI): aspects of the core-shell structure and reactions with inorganic species in water, J. Contam. Hydrol. 118 (2010) 96–104. [PubMed: 20889228]

[20]. Li X, Sotto A, Li J, Van der Bruggen B,Progress and perspectives for synthesis of sustainable antifouling composite membranes containing in situ generated nanoparticles, J. Membr. Sci 524 (2017) 502–528.

[21]. Greenlee LF, Hooker SA, Development of stabilized zero valent iron nanoparticles, Desalin. Water Treat 37 (2012) 114–121.

[22]. Zhang W.-x., Wang C-B, Lien H-L, Treatment of chlorinated organic contaminants with nanoscale bimetallic particles, Catal. Today 40 (1998) 387–395.

[23]. Schrick B, Blough JL, Jones AD, Mallouk TE, Hydrodechlorination of tri-chloroethylene to hydrocarbons using bimetallic nickel−iron nanoparticles, Chem. Mater 14 (2002) 5140–5147.

[24]. Feng J, Lim TT, Pathways and kinetics of carbon tetrachloride and chloroform reductions by nano-scale Fe and Fe/Ni particles: comparison with commercial micro-scale Fe and Zn, Chemosphere 59 (2005) 1267–1277. [PubMed: 15857638]

[25]. Lien H-L, Zhang W-X, Nanoscale Pd/Fe bimetallic particles: catalytic effects of palladium on hydrodechlorination, Appl. Catal. B 77 (2007) 110–116.

[26]. Xu J, Bhattacharyya D, Fe/Pd nanoparticle immobilization in microfiltration membrane pores: synthesis, characterization, and application in the dechlorination of polychlorinated biphenyls, Ind. Eng. Chem. Res 46 (2007) 2348–2359.

[27]. He F, Zhao D, Hydrodechlorination of trichloroethene using stabilized Fe-Pd nanoparticles: reaction mechanism and effects of stabilizers, catalysts and reaction conditions, Appl. Catal. B 84 (2008) 533–540.

[28]. Tee YH, Bachas L, Bhattacharyya D, Degradation of trichloroethylene and dichlorobiphenyls by iron-based bimetallic nanoparticles, J. Phys. Chem. C 113 (2009) 9454–9464.

[29]. Smuleac V, Bachas L, Bhattacharyya D, Aqueous-phase synthesis of PAA in PVDF membrane pores for nanoparticle synthesis and dichlorobiphenyl degradation, J. Membr. Sci 346 (2010) 310–317.

[30]. Xiao L, Isner AB, Hilt JZ, Bhattacharyya D, Temperature responsive hydrogel with reactive nanoparticles, J. Appl. Polym. Sci 128 (2013) 1804–1814. [PubMed: 30518988]

[31]. Hernández S, Lei S, Rong W, Ormsbee L, Bhattacharyya D, Functionalization of flat sheet and hollow fiber microfiltration membranes for water applications, ACS Sustain. Chem. Eng 4 (2015) 907–918. [PubMed: 29392097]

[32]. Aher A, Papp J, Colburn A, Wan H, Hatakeyama E, Prakash P, Weaver B, Bhattacharyya D, Naphthenic acids removal from high TDS produced water by persulfate mediated iron oxide functionalized catalytic membrane, and by nanofiltration, Chem. Eng. J 327 (2017) 573–583. [PubMed: 29398952]

[33]. Sagle AC, Ju H, Freeman BD, Sharma MM, PEG-based hydrogel membrane coatings, Polymer 50 (2009) 756–766.

[34]. Hernández S, Papp JK, Bhattacharyya D, Iron-based redox polymerization of acrylic acid for direct synthesis of hydrogel/membranes, and metal nanoparticles for water treatment, Ind. Eng. Chem. Res. 53 (2014) 1130–1142. [PubMed: 24954975]

[35]. Sarma R, Islam MS, Miller AF, Bhattacharyya D, Layer-by-layer-assembled laccase enzyme on stimuli-responsive membranes for chloro-organics degradation, ACS Appl. Mater. Interfaces 9 (2017) 14858–14867. [PubMed: 28397501]

[36]. Hwang S, Shao Q, Williams H, Hilty C, Gao YQ, Methanol strengthens hydrogen bonds and weakens hydrophobic interactions in proteins-a combined molecular dynamics and NMR study, J. Phys. Chem. B 115 (2011) 6653–6660. [PubMed: 21534580]

[37]. Khanlari S, Dubé MA, Effect of pH on poly(acrylic acid) solution polymerization, J. Macromol. Sci., Part A: Pure Appl. Chem 52 (2015) 587–592.

[38]. Gui M, Ormsbee LE, Bhattacharyya D, Reactive functionalized membranes for polychlorinated biphenyl degradation, Ind. Eng. Chem. Res 52 (2013) 10430–10440. [PubMed: 24954974]

[39]. Gui M, Papp JK, Colburn AS, Meeks ND, Weaver B, Wilf I, Bhattacharyya D, Engineered iron/iron oxide functionalized membranes for selenium and other toxic metal removal from power plant scrubber water, J. Membr. Sci 488 (2015) 79–91.

[40]. Wan H, Briot NJ, Saad A, Ormsbee L, Bhattacharyya D, Pore functionalized PVDF membranes with in-situ synthesized metal nanoparticles: material characterization, and toxic organic degradation, J. Membr. Sci. 530 (2017) 147–157.

[41]. Nielsen LE, Cross-linking-effect on physical properties of polymers, J. Macromol. Sci. Polym. Rev. 3 (1969) 69–103.

[42]. Kjøniksen A-L, Nyström B, Effects of polymer concentration and cross-linking density on rheology of chemically cross-linked poly(vinyl alcohol) near the gelation threshold, Macromolecules 29 (1996) 5215–5222.

[43]. Zhao F, Bi W, Zhao S, Influence of crosslink density on mechanical properties of natural rubber vulcanizates, J. Macromol. Sci. Part B: Phys 50 (2011) 1460–1469.

[44]. Ying L, Yu WH, Kang ET, Neoh KG, Functional and surface-active membranes from poly(vinylidene fluoride)-graft-poly(acrylic acid) prepared via RAFT-mediated graft copolymerization, Langmuir 20 (2004) 6032–6040. [PubMed: 16459627]

[45]. Ouyang Z-W, Chen E-C, Wu T-M, Thermal stability and magnetic properties of polyvinylidene fluoride/magnetite nanocomposites, Materials 8 (2015) 4553–4564. [PubMed: 28793456]

[46]. Moharram MA, Khafagi MG, Thermal behavior of poly(acrylic acid)–poly(vinyl pyrrolidone) and poly(acrylic acid)–metal–poly(vinyl pyrrolidone) complexes, J. Appl. Polym. Sci. 102 (2006) 4049–4057.

[47]. Xu J, Bhattacharyya D, Modeling of Fe/Pd nanoparticle-based functionalized membrane reactor for PCB dechlorination at room temperature, J. Phys. Chem. C 112 (2008) 9133–9144.

[48]. He F, Luo B, Yuan S, Liang B, Choong C, Pehkonen SO, PVDF film tethered with RGD-click-poly(glycidyl methacrylate) brushes by combination of direct surface-initiated ATRP and click chemistry for improved cytocompatibility, RSC Adv. 4 (2014) 105–117.

[49]. Kirwan LJ, Fawell PD, van Bronswijk W, In situ FTIR-ATR examination of poly (acrylic acid) adsorbed onto hematite at low pH, Langmuir 19 (2003) 5802–5807.

[50]. Groll J, Ademovic Z, Ameringer T, Klee D, Moeller M, Comparison of coatings from reactive star shaped PEG-stat-PPG prepolymers and grafted linear PEG for biological and medical applications, Biomacromolecules 6 (2005) 956–962. [PubMed: 15762665]

[51]. Zhang W, Wahlgren M, Sivik B, Membrane characterization by the contact angle technique, Desalination 72 (1989) 263–273.

[52]. Baek Y, Kang J, Theato P, Yoon J, Measuring hydrophilicity of RO membranes by contact angles via sessile drop and captive bubble method: a comparative study, Desalination 303 (2012) 23–28.

[53]. Choi J, Rubner MF, Influence of the degree of ionization on weak polyelectrolyte multilayer assembly, Macromolecules 38 (2005) 116–124.

[54]. Lützenkirchen J, van Male J, Leermakers F, Sjöberg S, Comparison of various models to describe the charge-pH dependence of poly(acrylic acid), J. Chem. Eng. Data 56 (2011) 1602–1612.

[55]. Swift T, Swanson L, Geoghegan M, Rimmer S, The pH-responsive behaviour of poly(acrylic acid) in aqueous solution is dependent on molar mass, Soft Matter 12 (2016) 2542–2549. [PubMed: 26822456]

[56]. Xiao L, Davenport DM, Ormsbee L, Bhattacharyya D, Polymerization and functionalization of membrane pores for water related applications, Ind. Eng. Chem. Res. 54 (2015) 4174–4182. [PubMed: 26074669]

[57]. Hadjipanayis CG, Bonder MJ, Balakrishnan S, Wang X, Mao H, Hadjipanayis GC, Metallic iron nanoparticles for MRI contrast enhancement and local hyperthermia, Small 4 (2008) 1925–1929. [PubMed: 18752211]

[58]. Yuvakkumar R, Elango V, Rajendran V, Kannan N, Preparation and characterization of zero valent iron nanoparticles, Dig. J. Nanomater. Biostruct. 6 (2011) 1771–1776.

[59]. Hudson R, Hamasaka G, Osako T, Yamada YM, Li C-J, Uozumi Y, Moores A, Highly efficient iron (0) nanoparticle-catalyzed hydrogenation in water in flow, Green Chem. 15 (2013) 2141–2148.

[60]. Gui M, Smuleac V, Ormsbee LE, Sedlak DL, Bhattacharyya D, Iron oxide nanoparticle synthesis in aqueous and membrane systems for oxidative degradation of trichloroethylene from water, J. Nanopart. Res. 14 (2012) 861.

[61]. Borchert H, Shevchenko EV, Robert A, Mekis I, Kornowski A, Grübel G, Weller H, Determination of nanocrystal sizes: a comparison of TEM, SAXS, and XRD studies of highly monodisperse CoPt3 particles, Langmuir 21 (2005) 1931–1936. [PubMed: 15723491]

[62]. Huang Q, Shi X, Pinto RA, Petersen EJ, Weber WJ, Jr., Tunable synthesis and immobilization of zero-valent iron nanoparticles for environmental applications, Environ. Sci. Technol. 42 (2008) 8884–8889. [PubMed: 19192813]

[63]. He F, Zhao D, Manipulating the size and dispersibility of zerovalent iron nanoparticles by use of carboxymethyl cellulose stabilizers, Environ. Sci. Technol 41 (2007) 6216–6221. [PubMed: 17937305]

[64]. Zhu B-W, Lim T-T, Catalytic reduction of chlorobenzenes with Pd/Fe nanoparticles: reactive sites, catalyst stability, particle aging, and regeneration, Environ. Sci. Technol 41 (2007) 7523–7529. [PubMed: 18044536]

[65]. Phenrat T, Saleh N, Sirk K, Tilton RD, Lowry GV, Aggregation and sedimentation of aqueous nanoscale zerovalent iron dispersions, Environ. Sci. Technol 41 (2007) 284–290. [PubMed: 17265960]

[66]. Greenlee LF, Torrey JD, Amaro RL, Shaw JM, Kinetics of zero valent iron nanoparticle oxidation in oxygenated water, Environ. Sci. Technol 46 (2012) 12913–12920. [PubMed: 23130994]

[67]. Islam MS, Rahman MM, Ilias S, Characterization of Pd–Cu membranes fabricated by surfactant induced electroless plating (SIEP) for hydrogen separation, Int. J. Hydrog. Energy 37 (2012) 3477–3490.

[68]. Choi H, Al-Abed SR, Agarwal S, Dionysiou DD, Synthesis of reactive nano-Fe/Pd bimetallic system-impregnated activated carbon for the simultaneous adsorption and dechlorination of PCBs, Chem. Mater. 20 (2008) 3649–3655.

[69]. Davis ME, Davis RJ, Fundamentals of Chemical Reaction Engineering, McGraw-Hill, New York, USA, 2003.

[70]. Chen NH, Process Reactor Design, Allyn and Bacon, Boston, USA, 1983.

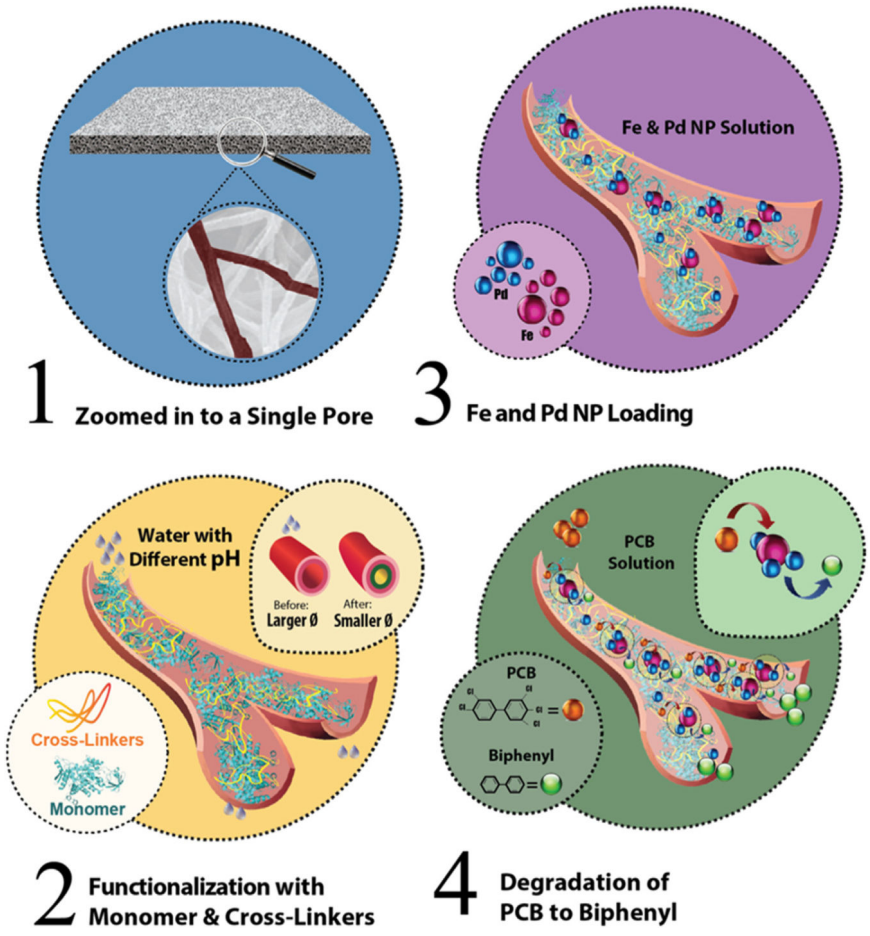

Fig. 1.

Schematic representation of step by step functionalization of the PVDF membrane and its use as a platform for PCB 126 degradation. (1) Zoomed image of PVDF pore is shown, (2) in-situ polymerization of membrane pores using monomer (acrylic acid (AA)) and cross-linker (N, N′-methylenebis (acrylamide) (MBA)). This causes the pore size to shrink and swell in different pH environment making it a pH responsive membrane, (3) Fe and Pd NPs are loaded inside the pores using a double ion exchange process by convective flow, (4) degradation of the PCB 126 solution to biphenyl using Pd-Fe-PAA-PVDF membrane.

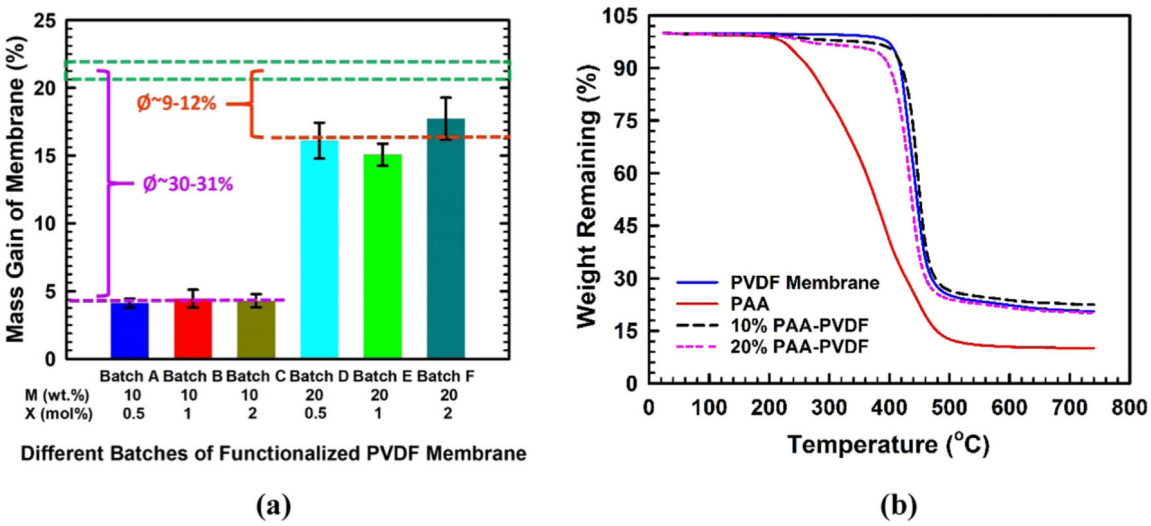

Fig. 2.

(a) Mass gain profile of different batches of functionalized PAA-PVDF membranes. The green dotted box is showing the maximum mass gain possible for PVDF membrane when all the pores are saturated with water with a base porosity (Ø) of 40%. For 10 wt% of monomer concentration approximately 30–31% porosity (Ø) remains after functionalization (shown in purple lines). For 20 wt% of monomer concentration almost 9–12% porosity (Ø) remains after functionalization (shown in orange lines) for permeation of water, (b) TGA thermograms of bare PVDF membrane (blue line), 10 wt% PAA-PVDF membrane (black line), 20 wt% PAA-PVDF membrane (green line) and PAA (redline). With an increase in PAA percentage in PVDF membrane the TGA curves are shifted towards PAA curve. (For interpretation of the references to color in this figure legend, the reader is referred to the web version of this article.)

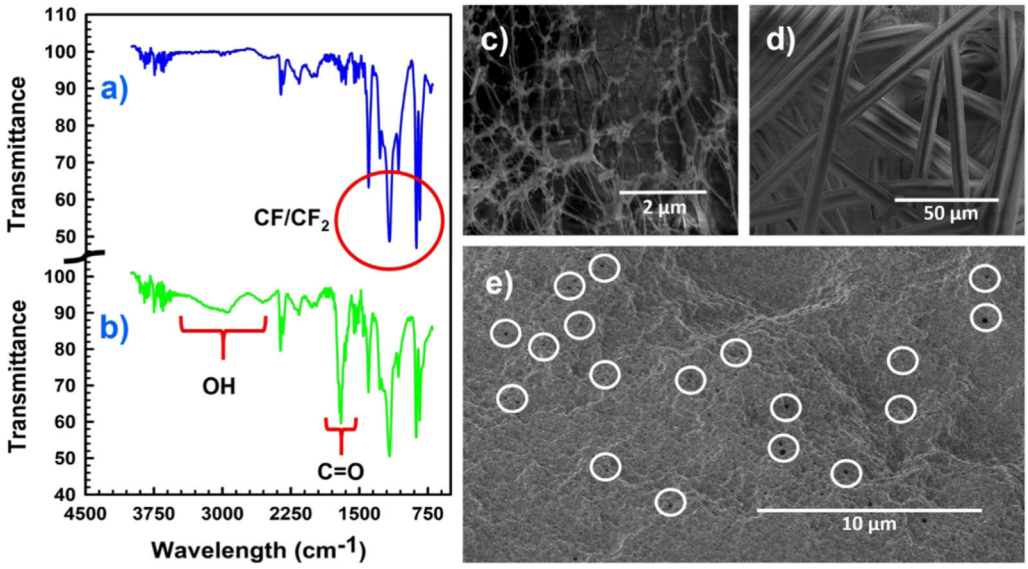

Fig. 3.

ATR-FTIR spectra of (a) blank PVDF membrane (blue line), (b) functionalized PAA-PVDF membrane (green line); SEM images of (c) a bare PVDF Membrane (top surface) showing the open pore networks, (d) back (polyester support materials) of the bare PVDF membrane, (e) functionalized PAA-PVDF membrane. The white circles encircled some of the pores remaining after functionalization.

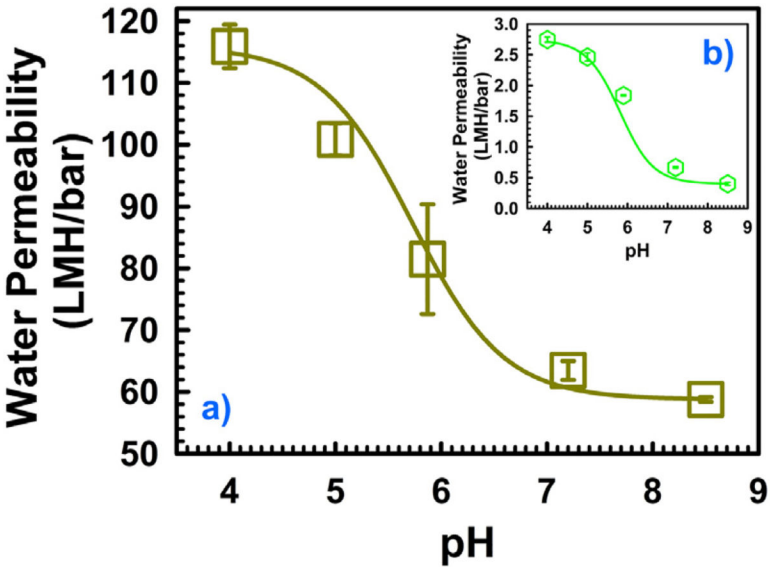

Fig. 4.

Typical water permeability profile of two different batches of functionalized membranes. (a) Batch C (10 wt% monomer and 2 mol% cross-linker), (b) batch F (20 wt% monomer and 2 mol% cross-linker). PAA-PVDF membrane area = 13.2 cm^2. T = 22–23 °C.

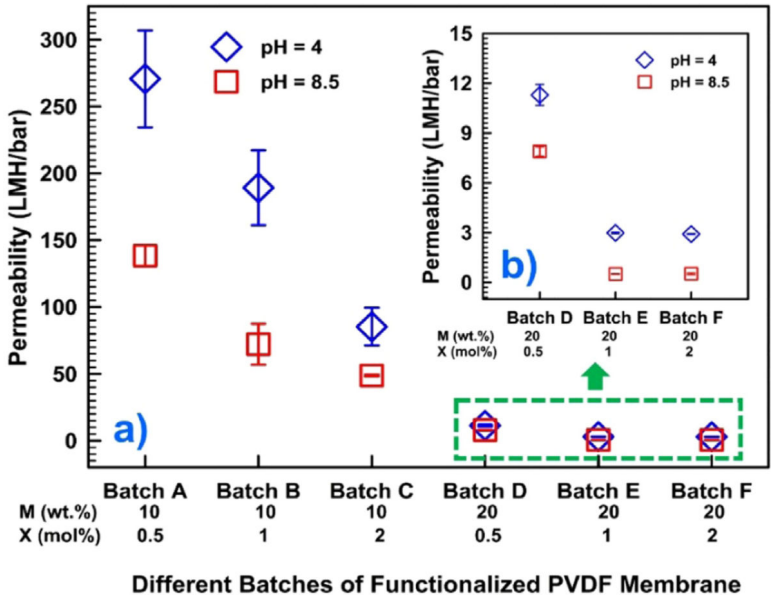

Fig. 5.

(a) Permeability data of six different batches of functionalized membranes at pH 4 and 8.5, (b) the green box in (a) are zoomed to show permeability data of three batches (D, E and F) with 20 wt% monomer concentrations. PAA-PVDF membrane area = 13.2 cm^2. T = 22–23 °C. (For interpretation of the references to color in this figure legend, the reader is referred to the web version of this article.)

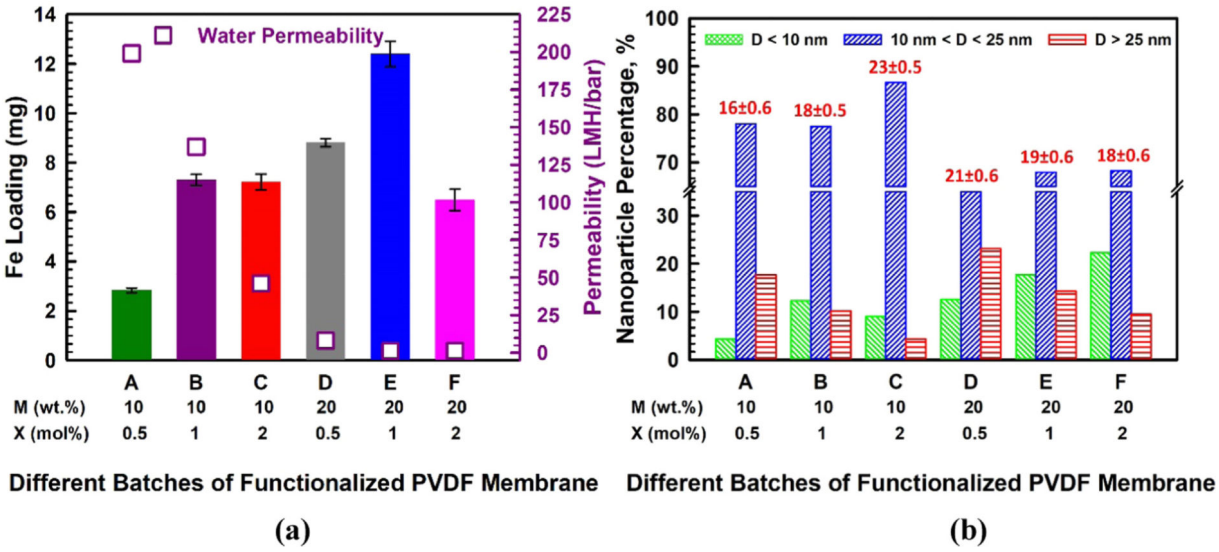

Fig. 6.

(a) Bar charts for the amount (mg) of Fe loading for different batches of functionalized membranes (membrane surface area = 13.2 cm^2, membrane volume = 0.225 cm^3), water permeability data during Fe^{2+} ion exchange are shown in right hand side y-axis, pH = 5.0–5.5, T = 22–24 °C, (b) particle size distribution and average particle size of different batches of functionalized membranes (total count is in the range of 300–400 NPs).

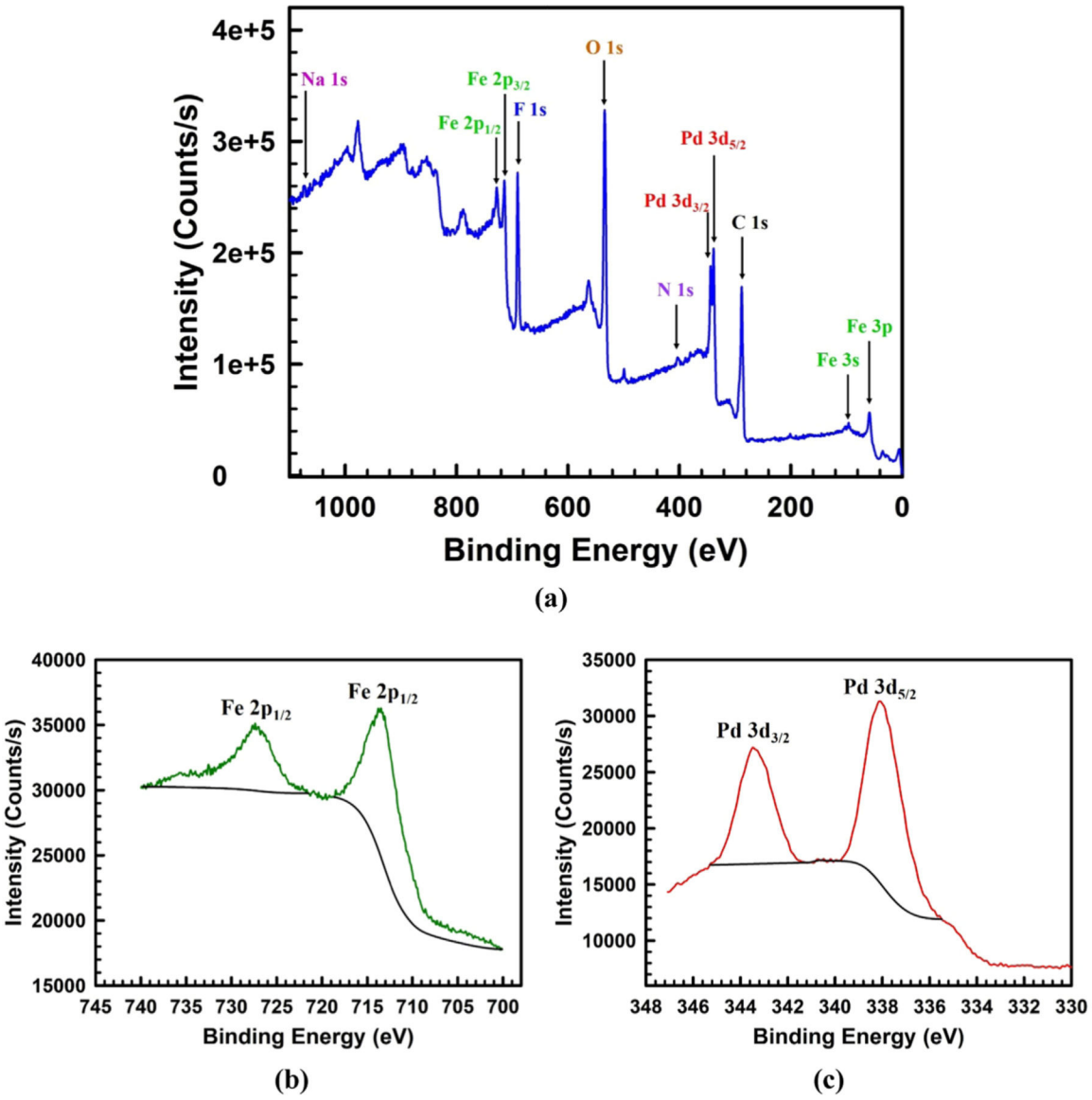

Fig. 7.

XPS spectrum of Pd-Fe-PAA-PVDF membrane. (a) Survery scan on the top surface of the membrane showing presence of the elements Pd, Fe, C, N, O, F and Na, (b) the doublet peaks for Fe 2p are assigned for Fe $2p_{3/2}$ and Fe $2p_{1/2}$ are due to presence of Fe°, (c) two doublet peaks are attributed to Pd $3d_{5/2}$ and Pd $3d_{3/2}$, associated with Pd° which is deposited on top of Fe NPs.

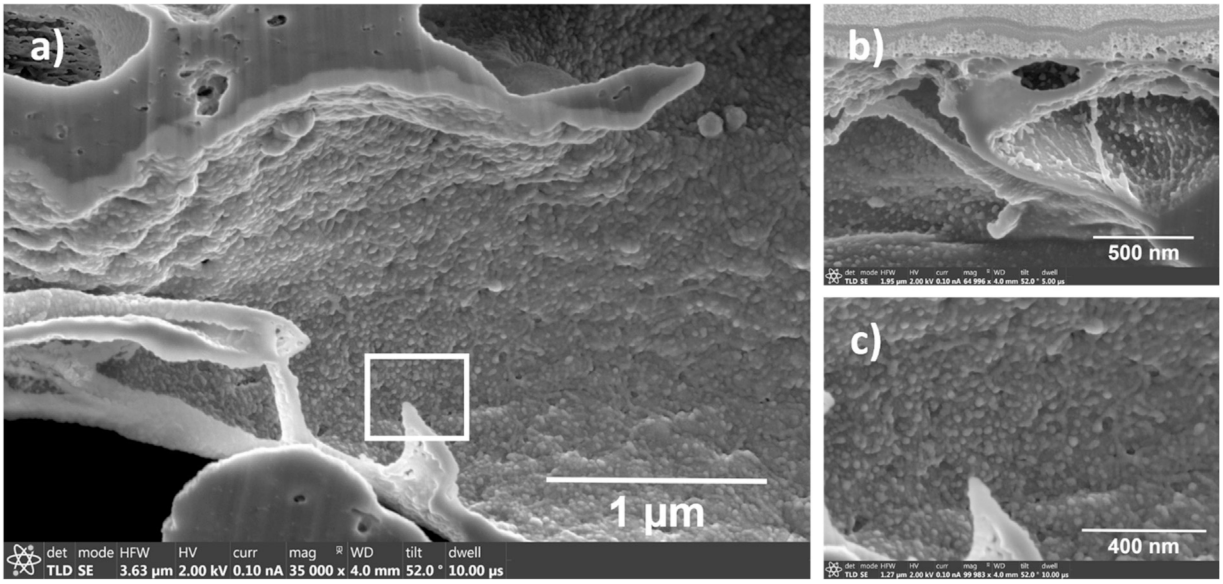

Fig. 8.

FIB-SEM images of Pd-Fe-PAA-PVDF membrane inner pores showing presence of Pd-Fe nanoparticles inside the pores. (a) Distance from the top surface in 3.196 µm (10 wt% of monomer, 1 mol% of cross-linker, 2.83 mg of Fe and 1 wt% of Pd), (b) distance from the top surface is 500 nm (10 wt% of monomer, 2 mol% cross-linker, 7.22 mg of Fe and 1 wt% of Pd), (c) zoomed image of the white squared box area of image (a) showing almost uniform Pd-Fe NPs are attached to pore wall evenly.

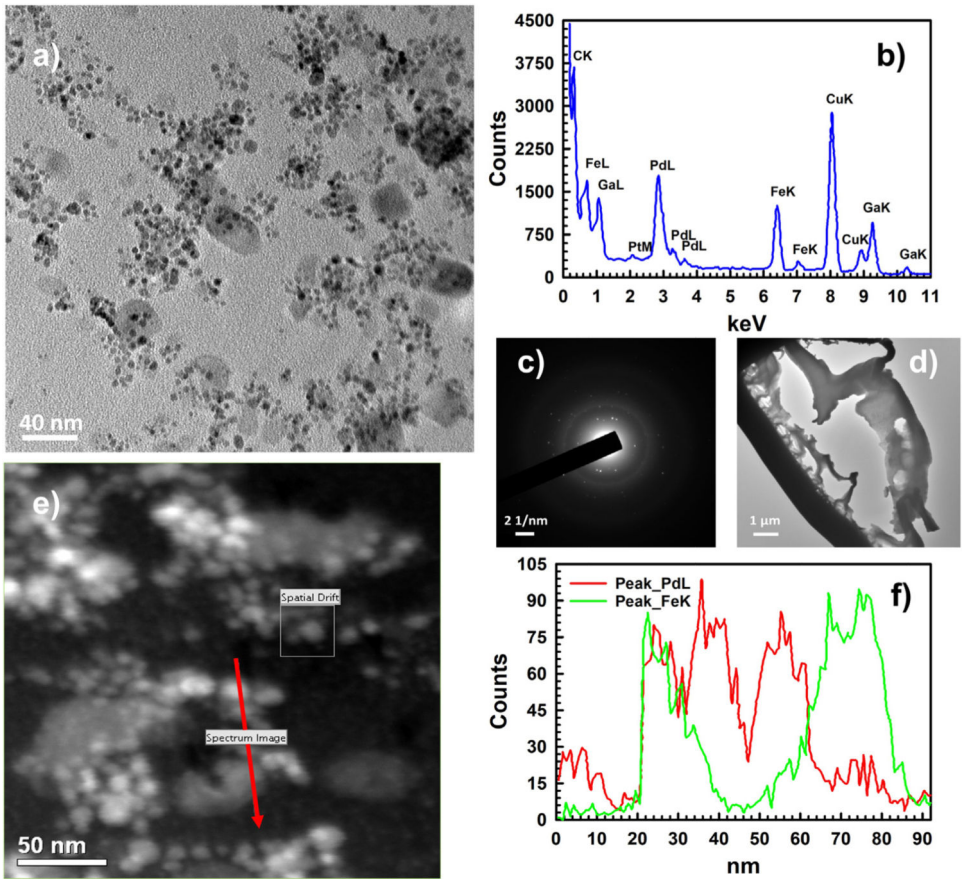

Fig. 9.

Inner surface (a thin lamella was prepared and lifted out from the inside with the help of FIB) of the Pd-Fe-PAA-PVDF membrane (20 wt% monomer and 1 mol% cross-linker) characterized by TEM, HRTEM and selected area electron diffraction (SAED). (a) A typical TEM image of the inner surface showing Pd/Fe nanoparticles (50 K magnification), (b) reproduced EDS spectrum showing peaks of Fe and Pd elements (100 K magnification). During preparation of lamella, gallium was used and signal confirms that. The copper signal is due to the sample holder made of copper, (c) the SAED pattern shows a diffraction halo (representing core carbon of the polymer) and multiple diffraction rings representing different phases of Pd and Fe elements (100 K magnification), (d) the lamella of the inner surface where HRTEM and SAED were conducted (2 K magnification), (e) survey image of inner surface conducted STEM mode (200 K magnification), (f) reproduced EDS signal profile for elemental mapping of the survey image (e) showing presence of Pd and Fe elements distribution in the high-lighted red arrowed line (200 K magnification).

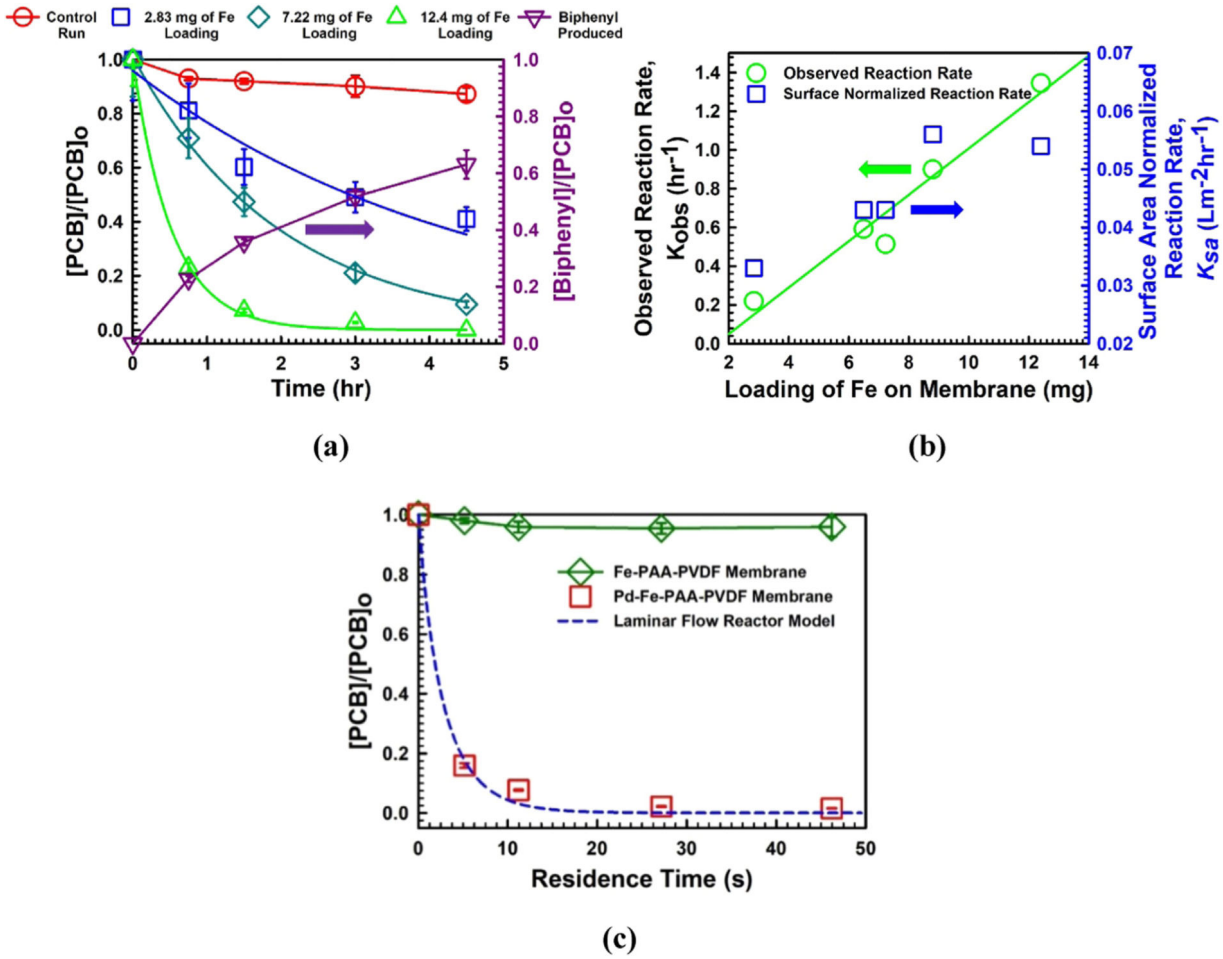

Fig. 10.

Results of PCB 126 degradation in different modes and kinetics study. (a) Batch study of PCB 126 degradation by Pd-Fe-PAA-PVDF membranes. $[PCB\ 126]_o$ ~ 15 μM, [Fe] = 0.71 g/L in solution, [Pd] ~ 1 wt% of Fe, pH = 5.6–5.7, T = 22–24 °C, (b) profile of observed reaction rate, K_{obs} (left y-axis) and surface area normalized reaction rate, K_{sa} (right y-axis) along with Fe loading on membrane effective surface area of 13.2 cm^2, (c) convective flow study of PCB 126 degradation by Pd-Fe-PAA-PVDF membranes. Fe-PAA-PVDF membrane served as blank control. Laminar flow reactor model was used for experimental data fitting (dashed blue line). Here, M = 20 wt%, X = 1 mol%, $[PCB]_o$ ~ 15 μM, Fe loading = 12.4 mg/13.2 cm^2 of membrane surface area, [Pd] ~ 1 wt% of Fe, pH = 5.6–5.7, T = 22–24 °C.

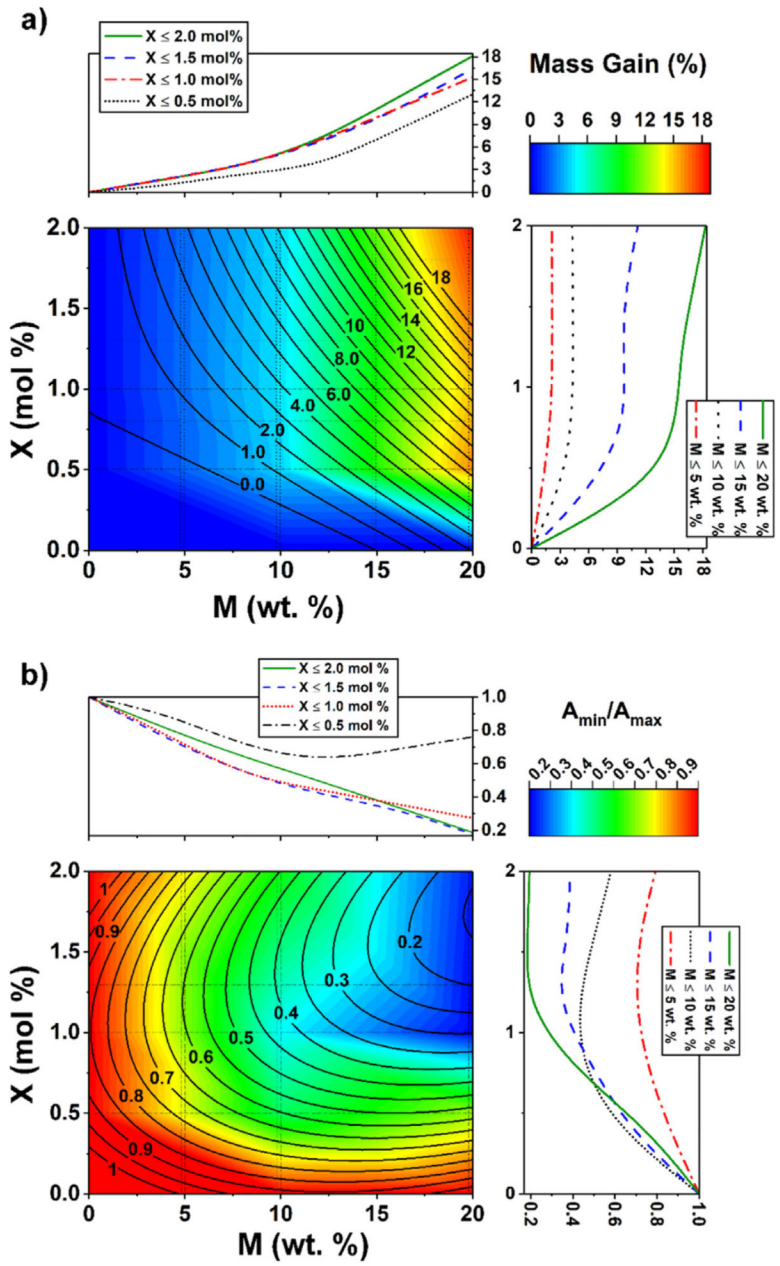

Fig. 11.

Response surfaces and depth profiles based on the concentrations of monomer, M (wt%) in x-axis and cross-linker, X (mol%) in y-axis. Experimental response surface is in color scale and fitted response is in contour. On the right and upper sides for X and M, respectively, a depth profile is shown maintaining the other factor constant at different intervals. (a) Mass gain (%), (b) permeability ratio, A_{min}/A_{max}. (For interpretation of the references to color in this figure legend, the reader is referred to the web version of this article.)

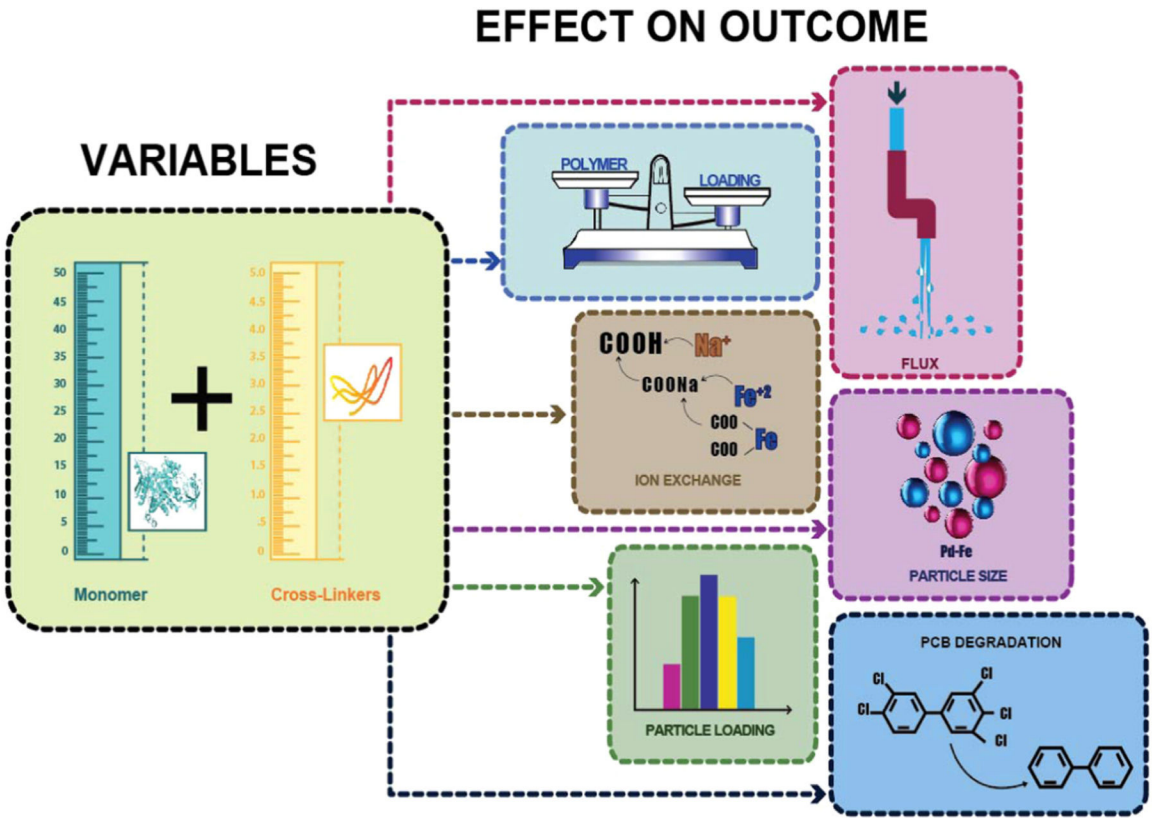

Scheme 1.

Graphical illustration depicting the specific aims of this work represented by block diagrams correlation of inputs (monomer and cross-linker concentrations) in left side and output variables (mass gain, water permeability, Ion exchange capacity, Fe metal loading and Pd-Fe nanoparticle size distribution and dechlorination of PCB 126 to biphenyl) in right side.

Table 1

Matrix of polymeric solution used for making different batches of functionalized PAA-PVDF membranes. Initiator (KPS) concentration is fixed to 1 mol% in all experiments and temperature of reaction is around 70–80 °C.

Batches (M, X)	Chemicals used for functionalization of membranes	
	Monomer (M) (AA = acrylic acid)	Cross-linker (X) (MBA = N, N′-methylenebis (acrylamide))
A (10, 0.5)	10 wt% of solution	0.5 mol% of AA
B (10, 1)	10 wt% of solution	1 mol% of AA
C (10, 2)	10 wt% of solution	2 mol% of AA
D (20, 0.5)	20 wt% of solution	0.5 mol% of AA
E (20, 1)	20 wt% of solution	1 mol% of AA
F (20, 2)	20 wt% of solution	2 mol% of AA